A novel CD44v6 targeting antibody fragment with improved tumor-to-blood ratio

K. SANDSTRÖM[1], A.K. HAYLOCK[1], D. SPIEGELBERG[2], F. QVARNSTRÖM[3], K. WESTER[4] and M. NESTOR[1,2]

[1]Department of Surgical Sciences, Unit of Otolaryngology and Head and Neck Surgery, [2]Department of Radiology, Oncology and Radiation Sciences, Unit of Biomedical Radiation Sciences, [3]Department of Radiology, Oncology and Radiation Sciences, Unit of Oncology, [4]Department of Immunology, Genetics and Pathology, Uppsala University, Uppsala, Sweden

Abstract. The chimeric monoclonal antibody U36 (cMAb U36) recognizes the CD44v6 antigen. Its potential as a radioimmunotargeting agent, as well as its safety, has been shown in previous studies in head and neck cancer patients. However, intact MAbs have long circulation time in the blood and tumor targeting may also be hampered due to the slow and incomplete diffusion into solid tumors. In comparison, smaller monovalent Fab' and divalent F(ab')$_2$ fragments are expected to exhibit shorter circulating half-lives, better tumor penetration and are thus more likely to yield better imaging results. In this study, novel F(ab')$_2$ and Fab' fragments from cMAb U36 were radiolabeled with ^{125}I and the characteristics of the conjugates *in vitro* were examined. The biodistribution of the conjugates were then evaluated in nude mice bearing CD44v6-expressing xenograft tumors. Furthermore, the penetration depth and distribution in tumor tissue was assessed by autoradiography in selected tumor samples. The *in vitro* experiments showed that the conjugates were stable and had intact affinity to CD44v6. The biodistribution study demonstrated superior tumor-to-blood ratio for the novel cMAb U36 fragment ^{125}I-F(ab')$_2$ compared with both the intact MAb and the monovalent fragment form. Autoradiography also revealed better tumor penetration for ^{125}I-F(ab')$_2$. This study demonstrates that the use of antibody fragments may improve radioimmunotargeting and possibly improve the management of head and neck malignancies.

Correspondence to: Dr Karl Sandström, Department of Surgical Sciences, Unit of Otolaryngology and Head and Neck Surgery, Uppsala University, Uppsala, Sweden
E-mail: karl.sandstrom@surgsci.uu.se

Introduction

Squamous cell carcinomas in the head and neck (HNSCC) present a major challenge worldwide. Nearly two thirds of patients present with advanced disease and less than one third of these patients are eventually cured. Despite significant improvements in surgery, radiation and chemotherapy, long-term survival rates for patients with advanced-stage HNSCC have not increased significantly in the past 30 years (1).

The presence or absence of lymphatic and distant metastases has a major impact on the preferred treatment and expected survival (2). FDG-PET, in addition to morphological diagnostics, is a valuable tool in the management of head and neck cancers, being superior to CT and MRI in the staging of lymph nodes (3). It is also valuable in the investigation of patients with unknown primary, e.g., patients presenting only with neck mass. In addition, FDG-PET is used for follow-up after treatment when searching for recurrent disease or metastasis (3-5). However, FDG-PET has some inherent problems. It shows metabolism of glucose and will hence result in false positive results in benign lymphadenitis or after treatment (6). A more tumor specific method such as radioimmunotargeting, PET or SPECT with radiolabeled antibodies directed against tumor cell-surface markers, may improve the management of patients with head and neck malignancies. Radioimmunotargeting combines the high sensitivity and resolution of a PET or SPECT camera, with the tumor specificity of an antibody or antibody fragment.

One of the most extensively studied targets for radioimmunotargeting of HNSCC is the CD44 splice variant v6 (CD44v6). This antigen has been proposed to be involved in aggressive tumor behavior (7), as a tumor-metastasis-promoting protein (8) and is associated with worse prognosis in several cancers including HNSCC (9). Homogeneous expression has been observed in many primary squamous cell carcinomas including their corresponding metastases. In normal tissue the expression is restricted to a subset of epithelia (10,11).

The chimeric monoclonal antibody U36 (cMAb U36) recognizes the CD44v6 antigen (12), and the potential as a radioimmunotargeting agent as well as its safety have been shown in previous imaging studies in head and neck cancer

patients (13,14). Clinical therapy studies have demonstrated favorable pharmacokinetics and promising results with radio-labeled cMAb U36, as well as with a fully humanized version, BIWA-4, binding to an overlapping epitope in the v6 domain (15,16).

For successful imaging, a targeting agent should rapidly find its target and bind with high specificity. In order to get high tumor-to-organ uptake ratios and contrast to surrounding tissue, the unbound fraction should be rapidly cleared from blood and excreted. Intact antibodies with a molecular weight of ~150 kDa have long circulation times in blood, ranging from a few days to weeks, due to slow plasma clearance. Tumor targeting may also be hampered because of the slow and incomplete diffusion into solid tumors (17,18). In comparison, the smaller monovalent Fab' (~50 kDa) and the divalent $F(ab')_2$ (~100 kDa) fragments derived from the parent antibody are expected to exhibit shorter circulating half-lives, better tumor penetration, and are thus more likely to yield better imaging results (19,20). To our knowledge, CD44v6-binding antibody fragments have never before been investigated as radioimmunotargeting molecules.

In this study the novel $F(ab')_2$ and Fab' fragments derived from cMAb U36 were radiolabeled with ^{125}I and the conjugates were first characterized *in vitro* for binding specificity, affinity, as well as yield, purity and stability of radiolabelling. The biodistribution of radiolabeled cMAb U36 and its $F(ab')_2$ and Fab' fragments was then evaluated in nude mice with CD44v6-expressing UT-SCC7 HNSCC tumors. Furthermore, the CD44v6 expression in these tumors was confirmed with immunohistochemistry, and the penetration depth and distribution of the conjugates in tumor tissue was assessed by autoradiography in selected tumor samples.

Materials and methods

Cell line. For the *in vitro* and *in vivo* experiments, the CD44v6 expressing head and neck squamous carcinoma cell line UT-SCC7 (kindly provided by Dr R. Grenman, Turku University Central Hospital, Finland) was used. UT-SCC7 cells were cultured in Dulbecco's modified Eagle's medium (DMEM), supplemented with 5 ml non-essential amino acids, 10% fetal calf serum, 2 mM L-glutamine and antibiotics (100 IU penicillin and 100 μg/ml streptomycin); referred to as complete medium. Cells were incubated at 37˚C in an atmosphere containing humidified air with 5% CO_2. Cells used in *in vitro* experiments were detached with trypsin-EDTA solution at 37˚C and seeded in separate dishes or flasks used for experiments 2-3 days prior to the studies.

Antibody and antibody fragments. The chimeric IgG1 monoclonal antibody U36 (cMAb U36), kindly provided by Dr G. van Dongen (VU University Medical Center, Amsterdam), recognizes the splice variant v6 of the membrane glycoprotein CD44. Selection and production of the antibody has been described previously (12,21). The antibody was supplied in citrate buffer, and separated upon arrival by size-exclusion chromatography on a NAP-5 column (Amersham Biosciences, Uppsala, Sweden) pre-equilibrated with purified (MilliQ) water. It was then freeze-dried and stored at -20˚C.

Fragmentation of cMAb U36 to $F(ab')_2$ and Fab' fragments was performed by GenScript (GenScriGenScript

USA Inc., Piscataway, NJ, USA). The products were purified using protein A and analyzed with non-reducing SDS-PAGE. Molecular weights were ~100 kDa [$F(ab')_2$] and ~50 kDa (Fab').

Labeling. Freeze-dried protein was dissolved in PBS and ^{125}I solution: 400 μg cMAb U36 (6 mg/ml, 6 MBq), 600 μg of U36-Fab' (5.33 mg/ml, 18 MBq) or 600 μg of $F(ab')_2$ (5 mg/ml, 24 MBq). The reaction was initiated by adding 120 μl chloramine-T (Sigma Aldrich) (8 mg/ml in MQ water) to each vial and stored on ice for 5 min. The reaction was quenched by adding 240 μl Na_2SO_5 (Merck) (8 mg/ml in MQ water). After labeling, the antibody and antibody fragments were separated from low-molecular-weight products (unbound ^{125}I) by size-exclusion chromatography on a NAP-5 column (Amersham Biosciences AB), pre-equilibrated with cell medium (Biocrom Kg).

For determination of stability over time, and purity of the labeled compound, instant thin-layer chromatography (ITLC) was performed 1, 24 and 48 h after the labeling procedure. Approximately 1 μl of the ^{125}I-U36, ^{125}I-Fab' and [125]I-$F(ab')_2$ solutions were placed on separate chromatography strips (Biodex) and put into 70% acetone, followed by measurements on a Cyclone Storage Phosphor System and analyzed using the OptiQuant image analysis software.

Affinity measurements. Kinetic affinity constants of ^{125}I-Fab' and [125]I-$F(ab')_2$ were determined as previously performed for the full length antibody conjugate ^{125}I-U36 (22), using saturation curves with a fixed amount of cells and different concentrations of radioimmunoconjugates. Three dishes per data point containing ~50,000 cells of UT-SCC7 cells were prepared with 100 μl complete culture medium. For some of the concentrations an excess of unlabeled antibody fragment in 100 μl complete culture medium was added to three additional dishes to determine non-specific binding. Concentrations varying between 0-100 nM of ^{125}I-labeled $F(ab')_2$ or Fab' in complete medium were added to the dishes. Cells were incubated on ice for 6 h. The incubation medium was then collected, and the dishes were washed six times with serum-free medium. The cells were detached with 100 μl trypsin-EDTA solution in 37˚C and re-suspended in 900 μl complete culture medium. Cell counting was performed on 0.5 ml of the cell suspensions. The radioactivity measurements were performed on the remaining cell suspension and the incubation medium in a gamma counter (1480 Wizard; Wallace Oy). Affinity calculations were performed using GraphPad Prism software.

Biodistribution. Tumor xenografts were formed by subcutaneous inoculation of 9x10⁶ UT-SCC7 cells, suspended in 400 μl injected medium, in the right posterior leg in 40 nude balb/c (nu/nu) female mice. The mice were housed in a controlled environment and fed *ad libitum*. Three weeks after injection, when the tumors had reached a size of ~0.5-1.0 g, biodistribution studies were performed. The experiments complied with current Swedish law and were performed with permission granted by the Uppsala Committee of Animal Research Ethics.

Thirty-six mice were divided into 3 groups, with 12 mice in each group. All animals were injected intravenously, via

the tail vein, with equimolar amounts of ^{125}I-labeled antibody or antibody fragments in 200 μl PBS. Group I received 10 μg (125 kBq) ^{125}I-labeled cMAb U36 (^{125}I-U36) per mouse, group II received 6.7 μg (93 kBq) ^{125}I-labeled F(ab')$_2$ [^{125}I-F(ab')$_2$] per mouse and group III received 3.4 μg (99.5 kBq) ^{125}I-labeled Fab' (^{125}I-Fab') per mouse.

After 16 h (n=12), 24 h (n=12) or 48 h (n=12) post injection, four mice from each group were euthanized with an overdose of a mixture of ketamine and xylazine given by intra-peritoneal injection followed by exsanguination via heart puncture. The tumor, blood, liver, spleen, kidneys, sub maxillary salivary glands, tongue, thyroid (en bloc with larynx), femur bone (including bone marrow) and skin were excised and weighed. One tumor from each treatment group and time point (9 tumors totally) was prepared for immunohistochemistry. The radioactivity content was measured in a gamma counter. For each group of animals, 3 injection standards of ^{125}I-U36, ^{125}I-F(ab')$_2$ and ^{125}I-Fab', respectively, were measured for radioactivity and the mean injected dose was calculated. The individual injected activity for each mouse was calculated as: injection standard - residual activity in the syringe - activity in tail. Radioactivity uptake in the organs was calculated as percent of injected dose per gram of tissue (% ID/g). For the thyroid, the uptake was calculated as percent of injected activity per organ. The tumor-to-organ ratio was calculated as activity/g$_{tumor}$ divided by activity/g$_{organ}$. See section on statistical analyses.

Three mice were injected intravenously with approximately seven times higher dose of radioimmunoconjugate; 68, 45 and 23 μg of ^{125}I-U36, ^{125}I-F(ab')$_2$ and ^{125}I-Fab', respectively. The mice were euthanized, as described above, 24 h post injection and the tumors were prepared for immunohistochemistry and autoradiography.

Immunohistochemistry and autoradiography. After radioactivity measurements and weighing, selected tumors were fixed in 10% buffered formalin and paraffin-embedded. Three consequent 10-μm sections from each tumor were mounted onto glass slides. The slides were heat-fixed overnight at 60°C, deparaffinized in xylene and hydrated in graded alcohols. The tumor slides were then processed for either autoradiography, immunohistochemistry with primary CD44v6 antibody or Mayer's hematoxylin counterstain.

Immunohistochemistry (IHC) was performed on nine tumors from the biodistribution study and all three high-dose tumors, essentially as previously described (23). After deparaffinization the slides were blocked for endogenous peroxidase in 0.3% hydrogen peroxide diluted in 95% ethanol. For antigen retrieval, a Decloaking Chamber® (Biocare Medical, Walnut Creek, CA) was used. Slides were immersed and boiled in Citrate Buffer®, PH6 (Lab Vision, Freemont, CA, USA) for 4 min at 125°C and then allowed to cool down to 90°C. Automated immunohistochemistry was done using an Autostainer 480 Instrument® (Lab Vision). Primary CD44v6 antibody (Chemicon, Temecula, CA, USA) was diluted 1:500 and a dextran polymer visualization system (UltraVision LP HRP Polymer®; Lab Vision) were incubated for 30 min each at room temperature and were developed for 2x5 min using Diaminobenzidine (Lab Vision) as chromogen. Incubation was

followed by rinsing in Wash Buffer® (Lab Vision). Slides were counterstained in Mayer's hematoxylin (Histolab, Gothenburg, Sweden) and coversliped using Pertex® (Histolab) as mounting medium.

Autoradiography (AR) was performed on all three high-dose tumors after removing paraffin with xylene and graded alcohol concentrations (99-10%). The slides were submerged in Kodak NTB photo emulsion (Eastman Kodak Co., Rochester, NY, USA) in the dark, dried and then stored at 4°C. After 2 months exposure, slides were developed in 1:1 Kodak D19 (Eastman Kodak Co.) for 3 min at room temperature. Development was stopped with 0.1% acetic acid for 10 sec followed by fixation in Kodak fixing solution (Eastman Kodak Co.) and finally rinsed in water for at least 5 min.

Images of the tumor slides were acquired with a Spot Insight CCD-camera (Diagnostic Instruments, Sterling Heights, MI) connected to a Nikon Eclipse E400 microscope (Nikon Corp., Tokyo, Japan) equipped with a x20 objective. The settings of the microscope and camera were optimized prior to image acquisition to ensure reproducible conditions throughout the image acquisition procedure. Using consecutively sectioned samples, IHC and eosin/pas staining could be employed to identify the blood vessels in the AR-staining. The AR-stained area was determined by digital image analysis algorithms implemented in Java™ and the Java Advanced Imaging platform. AR-labeled regions in the images were extracted by binary segmentation using a fixed gray level threshold. The software was designed so that uptake gradients could be determined along manually selected directions perpendicular to the identified blood vessels. Further processing by the software outlined five regions along the specified direction, each of size 20x40 μm, which assessed the gradient from the border of the vessel down to a total depth of 100 μm. An effort was made to measure individual gradients and to avoid inclusion of gradients from nearby blood vessels. AR-labeled area and total area of the selected regions were simultaneously recorded for each region, providing a measure of staining density at defined distances from the blood vessels. Uptake gradients were calculated by measuring a total of five gradients per sample. The uptake gradients were then normalized to the uptake values closest to the vessel (0-20 μm).

Statistical analyses. Statistical analyses were performed using GraphPad Prism Version 5.02 for Windows (GraphPad Software, Tumor Biol Inc., http://www.graphpad.com). Data from affinity studies were analyzed using non-linear regression analysis (one site binding) to calculate K_D. In the biodistribution studies, data are presented as the mean ± standard deviation (SD). The significance of differences between the groups in each time point was tested with One-way analysis of variance (ANOVA) with Tukey's multiple comparison test. Difference were considered statistically significant at $P<0.05$.

Results

Labeling. Labeling yields ranged between 42 and 71%. ITLC analyses showed that the radioimmunoconjugates had good purity, with values ranging from 94-100% and were stable for at least 2 days (data not shown).
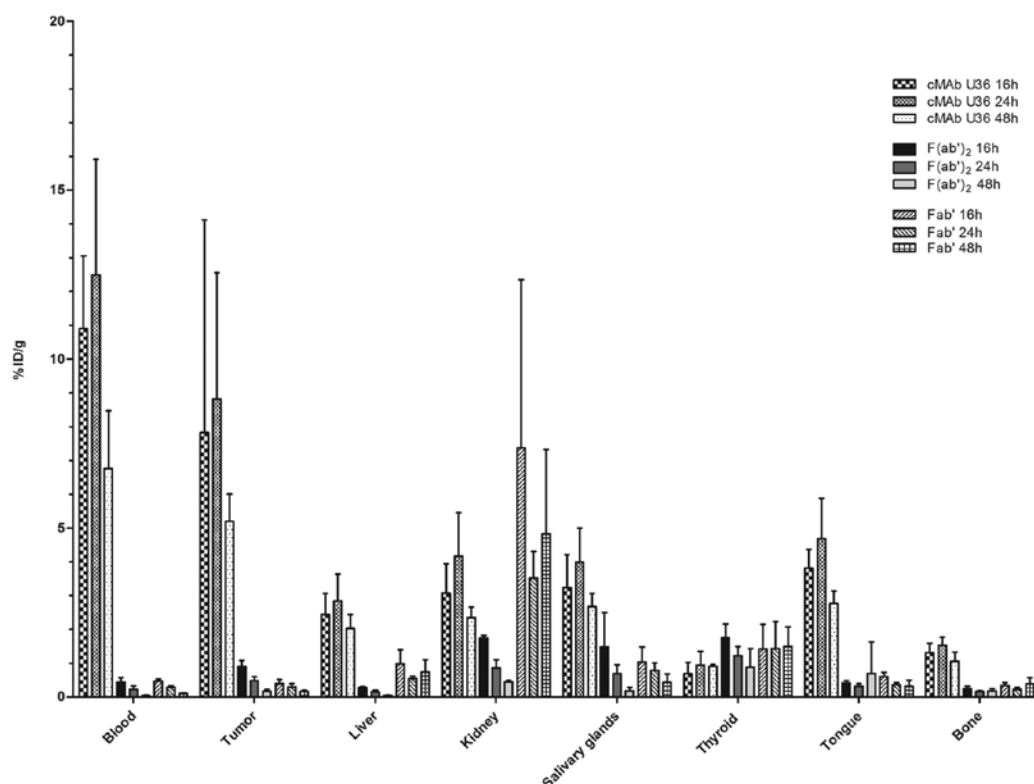
Figure 1. Biodistribution of ^{125}I-labeled cMAb U36, F(ab')$_2$ and Fab' in tumors and organs of UTSCC-7 xenograft bearing nude mice. Animals were sacrificed at 16, 24 or 48 h post injection. Data are expressed as percentages of injected activity per gram of tissue (% ID/g), except for the thyroid which is expressed as percentages of injected activity per organ. Error bars represent the standard deviation; n=4.

Affinity. The K_D for F(ab')$_2$ and Fab' to CD44v6 was 2.5×10^{-8} $\pm 4 \times 10^{-9}$ M and $3 \times 10^{-8} \pm 8 \times 10^{-9}$ M, respectively. Antigen specific binding of the fragments was clearly shown, as the binding of both antibody fragments were prevented by an excess of unlabeled antibody fragment (data not shown).

Biodistribution. The biodistribution data of ^{125}I-labeled cMAb U36, F(ab')$_2$ and Fab' in nude mice with UT-SCC 7 HNSCC xenografts are presented in Fig. 1. One mouse was excluded before the start of the experiment due to large tumor. ^{125}I-U36 displayed higher uptake than the fragments in the tumors as well as non-specific retention in all organs, apart from the kidney and thyroid, in all studied time points. The antibody fragments displayed a trend of maximum activity at the first time point. For cMAb U36 there was instead a trend of highest activity at the second time point, 24 h p.i. in both blood and tumor. In the kidney, the ^{125}I-F(ab')$_2$ uptake was lower than both ^{125}I-U36 and ^{125}I-Fab' at 24 h p.i. and in 48 h p.i. lower than ^{125}I-Fab'. In the thyroid there was no difference except at 16 h p.i. where ^{125}I-F(ab')$_2$ had higher uptake compared with ^{125}I-U36. The liver uptake of ^{125}I-F(ab')$_2$ at 48 h was lower than both ^{125}I-U36 and ^{125}I-Fab'. In the other organs including tumor there was no difference in measured activity between the fragments.

The tumor-to-organ uptake ratios of ^{125}I-U36, ^{125}I-F(ab')$_2$ and ^{125}I-Fab' in selected organs are presented in Fig. 2. The tumor-to-blood ratio of ^{125}I-F(ab')$_2$ was superior to ^{125}I-U36 already at 16 h and increased during the studied time period. At 48 h it was superior to both ^{125}I-U36 and ^{125}I-Fab'. The

tumor-to-salivary ratio showed a clear tendency of higher values for ^{125}I-U36, although only significant for 24 h [^{125}I-F(ab')$_2$ and ^{125}I-Fab'] and 48 h (^{125}I-Fab' only). In the tongue, no differences in tumor-to-organ ratio were seen between the different conjugates. The tumor-to-thyroid ratio was clearly better for ^{125}I-U36 compared with ^{125}I-F(ab')$_2$ and ^{125}I-Fab'. Also in the bone cMAb U36 displayed a higher tumor-to-organ ratio, although only significantly higher at 24 and 48 h post injection.

Immunohistochemistry and autoradiography. In Fig. 3 the images of Mayer's hematoxylin counterstain, IHC with primary CD44v6 antibody and AR of the high-dose tumors are presented. The IHC clearly showed that the tumor cells expressed CD44v6 in the cell membranes in all investigated tumors (n=12). In the images of autoradiography, the differences in total tumor uptake are obvious, with an intense staining in the ^{125}I-U36 treated tumor and weaker staining for ^{125}I-F(ab')$_2$ and ^{125}I-Fab' treated tumors. The uptake gradients presented in Fig. 4 demonstrates a pattern of more pronounced decline related to distance from the vessel in the ^{125}I-U36 treated tumor compared with the fragments. The antibody fragment treated tumors appeared to have a smaller decline in uptake, compared with the intact antibody.

Discussion

The aim of this study was to compare the biodistribution of ^{125}I-labeled cMAb U36 with its corresponding novel antibody
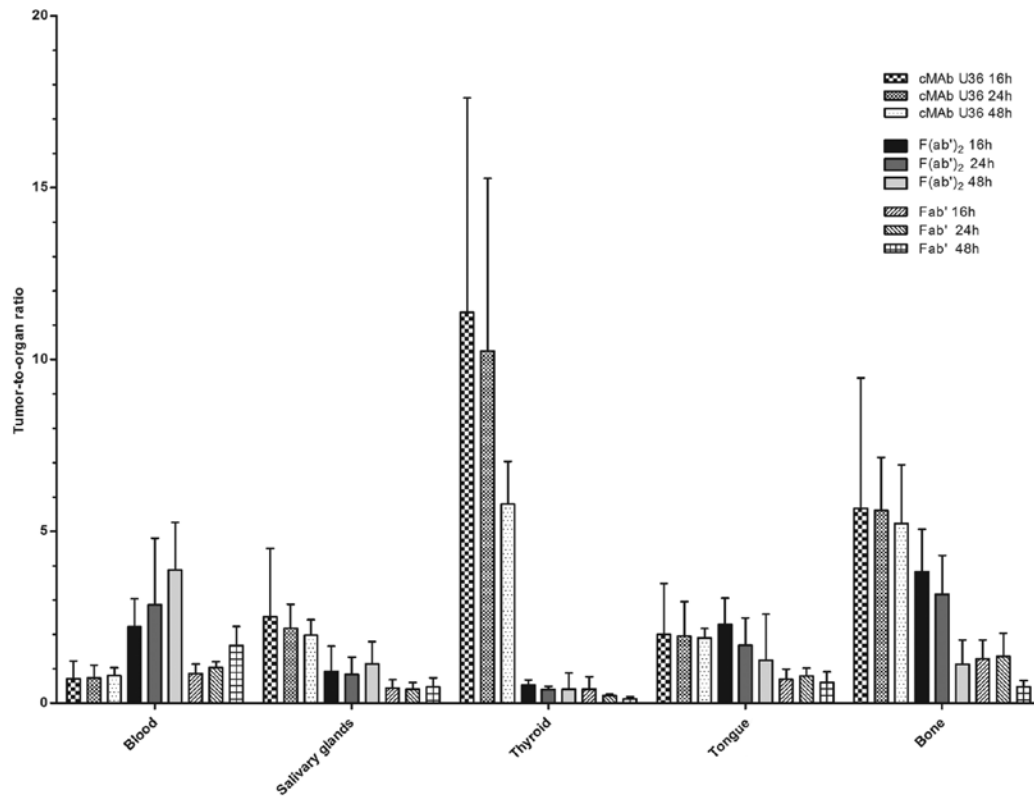
Figure 2. The tumor-to-organ ratio of ^{125}I-labeled cMAb U36, F(ab')$_2$ and Fab' in selected organs of UTSCC-7 xenografts bearing nude mice. Animals were sacrificed at 16, 24 or 48 h post injection. The tumor-to-organ ratio is expressed as activity/g$_{tumor}$ divided by activity/g$_{organ}$. Error bars represent the standard deviation; n=4.
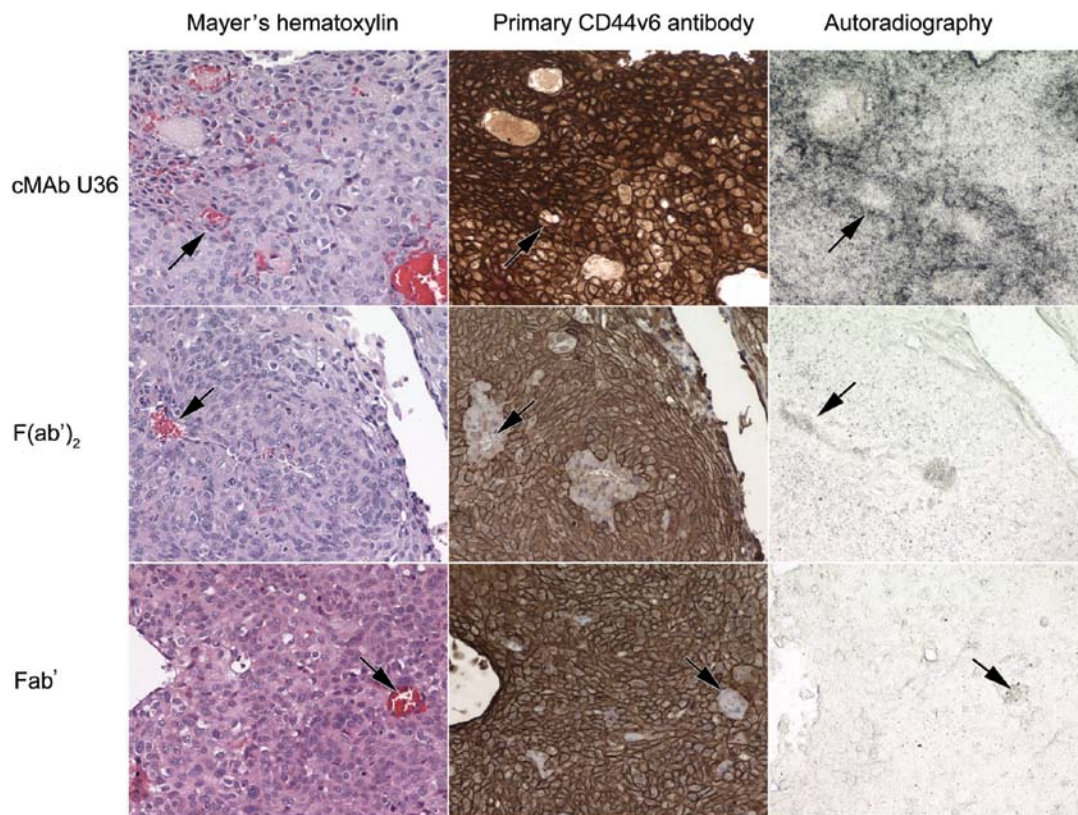

Figure 3. Images of 10-μm tumor sections from three mice injected with ^{125}I-labeled cMAb U36, F(ab')$_2$ or Fab'. Animals were sacrificed 24 h post injection. The tumor sections where cut consecutively, processed with either Mayer's hematoxylin counterstain, immunohistochemistry with primary CD44v6 antibody or autoradiography. The images were acquired with a Spot Insight CCD-camera with a x20 objective. Arrows indicate identified blood vessels.
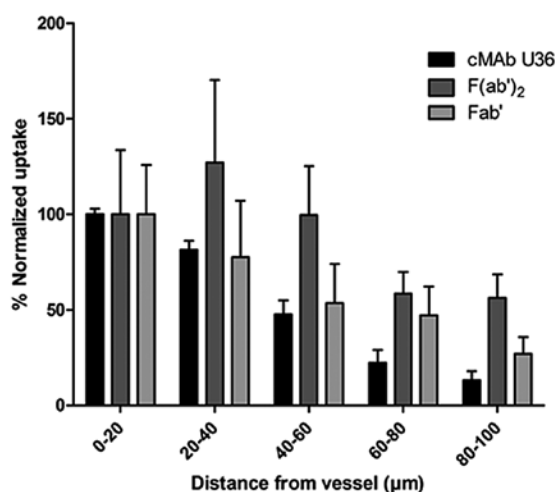
Figure 4. The uptake gradients normalized to the uptake values closest to the identified blood vessel (0-20 μm). Normalized uptake gradients were acquired from autoradiography stained 10-μm tumor sections of three mice injected with ^{125}I-labeled cMAb U36, F(ab')$_2$ or Fab'. Animals were sacrificed 24 h post injection. Error bars represent the standard deviation; n=5.

fragments F(ab')$_2$ and Fab'. This has, to our knowledge, never before been reported for CD44v6-binding radioimmunotargeting molecules. For other targets, enzymatically derived divalent F(ab')$_2$ and monovalent Fab' fragments have shown promising results in animal studies (24-28) and clinical studies (29,30) and F(ab')$_2$ fragments against a different target in HNSCC (E48) has been shown to be equally effective as the parent antibody, in tumor and lymph node detection with planar gamma camera (31).

The chimeric monoclonal antibody U36 recognizes the CD44v6 antigen (12), which shows consistent expression in many primary squamous cell carcinomas but only in a subset of normal tissues (11). The potential of CD44v6 as a tumor radioimmunotargeting agent has been demonstrated in previous studies (13,32). Radioimmunotargeting offers the possibility of non-invasive receptor quantification. This might be valuable as a prognostic factor in primary HNSCC, since strong expression of the CD44 isoforms has been associated with advanced T stage and decreased disease-free survival (33).

Intact antibodies have some intrinsic weaknesses in solid tumor localization and penetration due to their size. The rate of extravasation is very low, dense extracellular matrix and high interstitial pressure also limits tumor penetration. Moreover, heterogeneous blood supply hampers the delivery to less perfused regions of a tumor (17,18). Smaller molecules are likely to exhibit superior extravasation and diffusion in intracellular space compared to their parental antibody (19,20). The AR data from the present study confirms this with a prominent decline in uptake of the intact antibody relative to the distance from blood vessel, Fig. 4. The divalent F(ab')$_2$ and monovalent Fab' had a smaller decline in uptake. However, these results should be regarded as merely descriptive, as only one tumor treated with each immunoconjugate form was investigated with AR. The IHC confirmed that all twelve investigated tumors expressed CD44v6, and strengthens the result from the *in vitro* studies, showing the antigen specific binding of the cMAb fragments (Fig. 3). However, homogeneous tumor

infiltration is not the main objective in imaging, provided that expression of surface molecules is enough to discriminate the target tissue from background activity. The total tumor uptake of smaller molecules as antibody fragments is usually lower due to the short circulating half-life in blood, despite the superior tumor tissue penetration. The short circulating half-life is also likely to cause lower uptake in normal tissue, resulting in higher tumor-to-organ ratios and contrast. As expected, the ^{125}I-labeled cMAb U36 excelled in delivering radioactivity to the tumors in this study. The maximum uptake value was more than twenty times higher at 24 h post injection compared to the labeled fragments (Fig. 1). The blood activity was also several orders higher, as well as the non-specific retention in the liver, spleen, salivary glands, tongue, bone and skin. The activity of ^{125}I-labeled cMAb U36 in the blood, liver, kidney and spleen were in the same magnitude as previously reported with ^{124}I-labeled cMAb U36 (34). However, the contrast between tumor and surrounding tissue is of higher importance for imaging purposes than total tumor uptake. Both PET and SPECT are dynamic techniques, and the time between injection of agent and imaging can be altered to optimize imaging. Despite poorer tumor uptake, the highest tumor-to-blood ratio was achieved with ^{125}I-F(ab')$_2$, due to faster blood clearance and less blood activity compared with the intact antibody (Fig. 2). Similar results have been reported for ^{131}I-labeled antibody fragments against a different epitope (35). In the present study, ^{125}I-F(ab')$_2$ reached a maximum tumor-to-blood ratio at 48 h post injection, almost five times higher compared with ^{125}I-U36. However, already at 16 h p.i. the tumor-to-blood ratio was above two, enough for imaging. ^{125}I-F(ab')$_2$ showed greater tumor-to-blood ratio compared with ^{125}I-Fab' due to larger tumor uptake, since the blood activities were equal. The affinity to CD44v6 was equal for the fragments, the superior tumor uptake of F(ab')$_2$ is thus probably due to its divalent nature and increased avidity to the tumor cells, extending the retention in the tumor. The affinity of the fragments to CD44v6 was in the same range as previously reported for cMAb U36 (36).

For imaging in head and neck cancer, tumor-to-tissue contrast of muscle, salivary glands and thyroid and to some extent bone is important, in addition to the tumor-to-blood ratio. One should note that the uptake in mouse tissue is due to unspecific binding, since cMAb U36 only binds to human CD44v6. The transferability of the results to targeting HNSCC in humans is therefore somewhat limited, at least for organs with known CD44v6 expression as the epithelia of the oral cavity (10,11). However, a comparison between the tumor targeting capabilities of the studied conjugates can still be made. In the settings of this study there was no significant difference between the studied formats in the tongue. Nevertheless, there was a clear trend of higher tumor-to-tongue ratios with ^{125}I-U36 and ^{125}I-F(ab')$_2$, with values around two, rendering a possible contrast in imaging. In the salivary glands and bone ^{125}I-U36 demonstrated higher tumor-to-organ ratios compared to both fragments. The tumor-to-organ ratios of ^{125}I-F(ab')$_2$ and ^{125}I-Fab' in the thyroid were much lower than for ^{125}I-U36, mainly due to lower tumor uptake levels. The thyroid uptake was relatively high for both the intact antibody and its fragments. Thyroid and salivary gland uptake is most likely due to uptake of the free lipophilic iodine catabolites after proteolytic degradation of the immu-

noglobulin. Values in the same order have previously been reported for direct labeled ^{125}I antibody conjugates (22,37). By using other labeling strategies, thyroid and salivary gland uptake may possibly be reduced (22). The kidneys exhibited a relatively high uptake of ^{125}I-Fab'. High uptake of antibody fragments in the kidneys has been reported before (26,27) and is probably a result of reabsorption by the renal tubular cells and catabolism (38). ^{125}I-F(ab')$_2$ on the other hand had a lower uptake in the present study, most likely due to a size above the renal threshold (39). In head and neck cancer imaging renal uptake will be of less concern for delineation of the primary tumor and its metastases, although it may limit the amount of activity that can be administered to patients due to dose limiting toxicity to the kidneys.

The choice of radionuclide and the labeling method is an important aspect in successful radioimmunotargeting. To enable autoradiography of selected tumors we used a radionuclide with long half-life, ^{125}I, as a surrogate for radionuclides more suitable for imaging with PET or SPECT. Direct CAT labeling was used, as it is a fast and simple method with high immunoreactive fraction yield, rendering high specific activity. Further improvements in tumor-to-blood ratio could probably be achieved by using different labeling methods or radionuclides.

In conclusion, this biodistribution study in nude mice with CD44v6 expressing tumor xenografts demonstrated that the novel cMAb U36 fragment ^{125}I-F(ab')$_2$ had improved characteristics as a tumor imaging agent. The divalent ^{125}I-F(ab')$_2$ produced superior tumor-to-blood ratio compared with the intact MAb and the monovalent fragment form. This study shows that the use of antibody fragments could improve radioimmunotargeting of head and neck squamous cell carcinomas.

Acknowledgements

References

1. Pignon JP, Bourhis J, Domenge C and Designe L: Chemotherapy added to locoregional treatment for head and neck squamous-cell carcinoma: three meta-analyses of updated individual data. MACH-NC Collaborative Group. Meta-Analysis of Chemotherapy on Head and Neck Cancer. Lancet 355: 949-955, 2000.
2. Whitehurst JO and Droulias CA: Surgical treatment of squamous cell carcinoma of the oral tongue: factors influencing survival. Arch Otolaryngol 103: 212-215, 1977.
3. Connell CA, Corry J, Milner AD, et al: Clinical impact of, and prognostic stratification by, F-18 FDG PET/CT in head and neck mucosal squamous cell carcinoma. Head Neck 29: 986-995, 2007.
4. Fletcher JW, Djulbegovic B, Soares HP, et al: Recommendations on the use of ^{18}F-FDG PET in oncology. J Nucl Med 49: 480-508, 2008.
5. Brouwer J, Hooft L, Hoekstra OS, et al: Systematic review: accuracy of imaging tests in the diagnosis of recurrent laryngeal carcinoma after radiotherapy. Head Neck 30: 889-897, 2008.
6. Shreve PD, Anzai Y and Wahl RL: Pitfalls in oncologic diagnosis with FDG PET imaging: physiologic and benign variants. Radiographics 19: 61-77, 1999.
7. Terpe HJ, Storkel S, Zimmer U, et al: Expression of CD44 isoforms in renal cell tumors. Positive correlation to tumor differentiation. Am J Pathol 148: 453-463, 1996.
8. Gunthert U, Hofmann M, Rudy W, et al: A new variant of glycoprotein CD44 confers metastatic potential to rat carcinoma cells. Cell 65: 13-24, 1991.
9. Kainz C, Kohlberger P, Tempfer C, et al: Prognostic value of CD44 splice variants in human stage III cervical cancer. Eur J Cancer 31A: 1706-1709, 1995.
10. Heider KH, Mulder JW, Ostermann E, et al: Splice variants of the cell surface glycoprotein CD44 associated with metastatic tumour cells are expressed in normal tissues of humans and cynomolgus monkeys. Eur J Cancer 31A: 2385-2391, 1995.
11. Fox SB, Fawcett J, Jackson DG, et al: Normal human tissues, in addition to some tumors, express multiple different CD44 isoforms. Cancer Res 54: 4539-4546, 1994.
12. Schrijvers AH, Quak JJ, Uyterlinde AM, et al: MAb U36, a novel monoclonal antibody successful in immunotargeting of squamous cell carcinoma of the head and neck. Cancer Res 53: 4383-4390, 1993.
13. Borjesson PK, Jauw YW, Boellaard R, et al: Performance of immuno-positron emission tomography with zirconium-89-labeled chimeric monoclonal antibody U36 in the detection of lymph node metastases in head and neck cancer patients. Clin Cancer Res 12: 2133-2140, 2006.
14. De Bree R, Roos JC, Quak JJ, den Hollander W, Snow GB and van Dongen GA: Radioimmunoscintigraphy and biodistribution of technetium-99m-labeled monoclonal antibody U36 in patients with head and neck cancer. Clin Cancer Res 1: 591-598, 1995.
15. Colnot DR, Quak JJ, Roos JC, et al: Phase I therapy study of ^{186}Re-labeled chimeric monoclonal antibody U36 in patients with squamous cell carcinoma of the head and neck. J Nucl Med 41: 1999-2010, 2000.
16. Borjesson PK, Postema EJ, Roos JC, et al: Phase I therapy study with (186)Re-labeled humanized monoclonal antibody BIWA 4 (bivatuzumab) in patients with head and neck squamous cell carcinoma. Clin Cancer Res 9: S3961-S3972, 2003.
17. Jain RK: Physiological barriers to delivery of monoclonal antibodies and other macromolecules in tumors. Cancer Res 50: S814-S819, 1990.
18. Thurber GM, Zajic SC and Wittrup KD: Theoretic criteria for antibody penetration into solid tumors and micrometastases. J Nucl Med 48: 995-999, 2007.
19. Schmidt MM and Wittrup KD: A modeling analysis of the effects of molecular size and binding affinity on tumor targeting. Mol Cancer Ther 8: 2861-2871, 2009.
20. Covell DG, Barbet J, Holton OD, Black CD, Parker RJ and Weinstein JN: Pharmacokinetics of monoclonal immunoglobulin G$_1$, F(ab')$_2$, and Fab' in mice. Cancer Res 46: 3969-3978, 1986.
21. Brakenhoff RH, van Gog FB, Looney JE, van Walsum M, Snow GB and van Dongen GA: Construction and characterization of the chimeric monoclonal antibody E48 for therapy of head and neck cancer. Cancer Immunol Immunother 40: 191-200, 1995.
22. Nestor M, Persson M, Cheng J, et al: Biodistribution of the chimeric monoclonal antibody U36 radioiodinated with a closo-dodecaborate-containing linker. Comparison with other radioiodination methods. Bioconjug Chem 14: 805-810, 2003.
23. Paavilainen L, Wernerus H, Nilsson P, et al: Evaluation of monospecific antibodies: a comparison study with commercial analogs using immunohistochemistry on tissue microarrays. Appl Immunohistochem Mol Morphol 16: 493-502, 2008.
24. Behr TM, Blumenthal RD, Memtsoudis S, et al: Cure of metastatic human colonic cancer in mice with radiolabeled monoclonal antibody fragments. Clin Cancer Res 6: 4900-4907, 2000.
25. Burvenich IJG, Schoonooghe S, Blanckaert P, et al: Biodistribution and planar gamma camera imaging of ^{123}I- and ^{131}I-labeled F(ab')$_2$ and Fab fragments of monoclonal antibody 14C5 in nude mice bearing an A549 lung tumor. Nucl Med Biol 34: 257-265, 2007.
26. Massuger LF, Boerman OC, Corstens FH, et al: Biodistribution of iodine-125 and indium-111 labeled OV-TL 3 intact antibodies and F(ab')$_2$ fragments in tumor-bearing athymic mice. Anticancer Res 11: 2051-2057, 1991.
27. Khawli LA, Alauddin MM, Hu P and Epstein AL: Tumor targeting properties of indium-111 labeled genetically engineered Fab' and F(ab')$_2$ constructs of chimeric tumor necrosis treatment (chTNT)-3 antibody. Cancer Biother Radiopharm 18: 931-940, 2003.

28. Hoeben BA, Kaanders JH, Franssen GM, *et al*: PET of hypoxia with [89]Zr-labeled cG250-F(ab')$_2$ in head and neck tumors. J Nucl Med 51: 1076-1083, 2010.
29. Murray JL, Rosenblum MG, Zhang HZ, *et al*: Comparative tumor localization of whole immunoglobulin G anticarcinoembryonic antigen monoclonal antibodies IMMU-4 and IMMU-4 F(ab')$_2$ in colorectal cancer patients. Cancer 73: 850-857, 1994.
30. Willkomm P, Bender H, Bangard M, Decker P, Grunwald F and Biersack HJ: FDG PET and immunoscintigraphy with ^{99m}Tc-labeled antibody fragments for detection of the recurrence of colorectal carcinoma. J Nucl Med 41: 1657-1663, 2000.
31. De Bree R, Roos JC, Quak JJ, *et al*: Clinical imaging of head and neck cancer with technetium-99m-labeled monoclonal antibody E48 IgG or F(ab')$_2$. J Nucl Med 35: 775-783, 1994.
32. Borjesson PK, Jauw YW, de Bree R, *et al*: Radiation dosimetry of [89]Zr-labeled chimeric monoclonal antibody U36 as used for immuno-PET in head and neck cancer patients. J Nucl Med 50: 1828-1836, 2009.
33. Wang SJ, Wong G, de Heer AM, Xia W and Bourguignon LY: CD44 variant isoforms in head and neck squamous cell carcinoma progression. Laryngoscope 119: 1518-1530, 2009.
34. Fortin MA, Salnikov AV, Nestor M, Heldin NE, Rubin K and Lundqvist H: Immuno-PET of undifferentiated thyroid carcinoma with radioiodine-labelled antibody cMAb U36: application to antibody tumour uptake studies. Eur J Nucl Med Mol Imaging 34: 1376-1387, 2007.
35. Burvenich IJ, Schoonooghe S, Blanckaert P, *et al*: Biodistribution and planar gamma camera imaging of (123)I- and (131)I-labeled F(ab')(2) and Fab fragments of monoclonal antibody 14C5 in nude mice bearing an A549 lung tumor. Nucl Med Biol 34: 257-265, 2007.
36. Nestor M, Sundstrom M, Anniko M and Tolmachev V: Effect of cetuximab in combination with alpha-radioimmunotherapy in cultured squamous cell carcinomas. Nucl Med Biol 38: 103-112, 2011.
37. Fortin MA, Salnikov AV, Nestor M, Heldin NE, Rubin K and Lundqvist H: Immuno-PET of undifferentiated thyroid carcinoma with radioiodine-labelled antibody cMAb U36: application to antibody tumour uptake studies. Eur J Nucl Med Mol Imaging 34: 1376-1387, 2007.
38. Wochner RD, Strober W and Waldmann TA: The role of the kidney in the catabolism of Bence Jones proteins and immunoglobulin fragments. J Exp Med 126: 207-221, 1967.
39. Holechek MJ: Glomerular filtration: an overview. Nephrol Nurs J 30: 285-291, 2003.